Biochemical and Biophysical Research Communications 456 (2015) 737–742

Contents lists available at ScienceDirect

Biochemical and Biophysical Research Communications

journal homepage: www.elsevier.com/locate/ybbrc

Crystal structure of the *Locusta migratoria* odorant binding protein ☆

Jiangge Zheng [a], Junru Li [a], Lei Han [a,b], Yang Wang [a], Wei Wu [a], Xiaoxuan Qi [a], Ye Tao [d], Long Zhang [c], Ziding Zhang [a], Zhongzhou Chen [a,*]

[a] State Key Laboratory of Agrobiotechnology, China Agricultural University, Beijing 100193, China
[b] Tianjin Medical University Cancer Institute and Hospital, National Clinical Research Center of Cancer, Tianjin 300060, China
[c] Department of Entomology, China Agricultural University, Beijing 100193, China
[d] Beijing Synchrotron Radiation Facility, Institute of High Energy Physics, Chinese Academy of Sciences, Beijing 100049, China

ARTICLE INFO

Article history:
Received 29 November 2014
Available online 15 December 2014

Keywords:
Locusta migratoria
Odorant binding protein
Odorant perception
Crystal structure
Ligand binding mechanism

ABSTRACT

Locusta migratoria (Lmig) causes enormous losses to agricultural products, especially because it often infests the world with great swarms as locust plagues. Locusts find their plant hosts on which they feed through their olfactory system, in which odorant binding proteins (OBPs) play an important role. Previous study indicated that the amino acid sequences of LmigOBP showed low similarity to OBPs from other insect orders and we speculated that it might perform unique binding behavior. Here, we solved the first LmigOBP1 structure at 1.65 Å, which is a monomer in solution and disulfide bonds play a key role in maintaining its function. We show that LmigOBP1 possesses a unique seventh α-helix, which is located at the surface with strong interactions with the LmigOBP1 scaffold consisting of other six α-helices. Moreover, the seventh α-helix forms a wall of an "L" shaped internal hydrophobic cavity to accommodate linear ligands, which is consistent with the binding experiments. We also demonstrate that the ligand-binding pocket in LmigOBP1 is greatly different from that in the closest homologs mosquito OBPs. Taken together, this study provides a structural basis for designing small inhibitors to control locust.

1. Introduction

Locusta migratoria is a notorious worldwide agriculture pest. Owing to the great damage caused by locust, it is of enormous benefits to find a better way to prevent locusts' swarms. There are different approaches to control locust population, among which the use of semiochemicals appears environment-friendly.

Chemical signals play a pivotal role in insect fundamental behaviors. Thus, it is very effective to block the signaling pathway of olfactory system to limit the losses caused by locusts. In insects, there are a large number of 13–17 kDa, highly water-soluble OBPs [1], which occupy a central position in the signaling pathway and play numerous functions in many phases of odorant perception.

The remarkable similarities of insect OBPs make it possible to define a "classical OBPs" group, which have identical characteristics, including six or seven α-helices, three strictly conserved disulfide bridges and a hydrophobic binding pocket. However, mounting studies have demonstrated that insect OBPs have significant differences in ligand binding and release mechanisms. On the basis of insect OBPs' lengths, they are composed of long-chain OBPs (~160 residues), medium-chain OBPs (~120 residues) and short-chain OBPs (~100 residues).

To date, several structures of insect OBPs have been solved. The first solved structure was the silkworm *Bombyx mori* PBP (BmorPBP), in which there existed a pH-dependent conformational change for releasing ligand [2]. The following NMR structure proved that the C-terminal dodecapeptide segment of the acidic form of BmorPBP (pH 4.5) formed an additional helix in the protein core, occupied the corresponding pheromone-binding site and released ligands [3].

Aside from the above long-chain OBPs structures, there are several structures of medium-chain OBPs reported, including *Anopheles gambia* OBP1 (AgamOBP1) [4], AgamOBP7 [5] and *Culex quinquefasciatus* OBP1 (CquiOBP1) [6], in which the C-terminal extensions are locked by a hydrogen bond triad composed of the last residue and two other residues (Tyr and His). The hydrogen bond triad would be disrupted at lower pH, leading to the C-terminal loop move away from the binding pocket and the "lid" open.

Abbreviations: PBP, pheromone binding protein; Lmig, *Locusta migratoria*; OBP, odorant binding protein; DTT, dithiothreitol; PEG, polyethylene glycol; CD, circular dichroism; 1-NPN, N-phenyl-1-naphthylamine.

☆ *Accession codes:* The structure coordinates have been deposited to the Protein Data Bank with accession codes 4PT1.

* Corresponding author.
E-mail address: chenzhongzhou@cau.edu.cn (Z. Chen).

http://dx.doi.org/10.1016/j.bbrc.2014.12.048
0006-291X/

LmigOBP1 is vital for locusts to percept environmental chemical signals. Despite its key role as a drug target for insect control, no three-dimensional structural information has been reported. Here, we reported the first X-ray structure of LmigOBP1 at 1.65 Å. The overall structure resembles the "classical OBPs" fold. A unique binding pocket with a long hydrophobic channel and a special C-terminal helix are found. And pH changes have no obvious effect on LmigOBP1. Our results provide a useful structural basis for further effective locust control.

2. Materials and methods

2.1. Protein cloning, expression and purification

The cDNA encoding residues 1–131 of *LmigOBP1* was cloned into the pET-22b periplasmic expression vector between *Nco* I and *Xho* I restriction sites. The correct plasmid was transformed into BL21 (DE3) cells. Cells were grown at 37 °C till OD_{600} reached 0.6 and protein expression was induced with 0.4 mM isopropyl β-D-thiogalactopyranoside (IPTG) at 18 °C for 16 h. Cells were harvested by centrifuging at 4000 rev min^{-1} for 10 min, and then resuspended in a lysis buffer containing 100 mM Tris–HCl pH 8.0, 2 mM EDTA and 20% sucrose. The cell lysates were centrifuged at 13,000 rev min^{-1} for 10 min at 4 °C. The cell precipitates were resuspended again in 20 mM Tris–HCl pH 8.0 and 5 mM $MgCl_2$, and were stirred on the ice for 10 min. Finally, the cell lysates were centrifuged at 13,000 rev min^{-1} for 30 min. The clear supernatant was loaded onto a Q-Sepharose (GE Healthcare) column equilibrated with buffer containing 20 mM Tris–HCl pH 8.0 and eluted with a 0–300 mM NaCl gradient. The eluted protein was further purified by size-exclusion chromatography. Peak fractions were collected and analyzed by SDS–PAGE.

2.2. Protein crystallization and data collection

The purified protein was concentrated to 10 mg/ml in 20 mM Tris–HCl pH 8.0, 150 mM NaCl. Initial crystallization trials were performed at different temperature using the vapor-diffusion method. The crystallization conditions used were from commercial crystallization kits (Hampton Research, Qiagen, XtalQuest and Emerald BioSystems). After several days, crystals grew in a lot of PEG conditions as needles. After extensive optimization, large high-quality LmigOBP1 crystals were finally obtained in a buffer comprising 25% PEG3350, 0.2 M ammonium acetate and 0.1 M Bis–Tris pH 6.2, after six months at 4 °C. The crystals were frozen for data collection in the above crystallization buffer containing 15% glycerol.

Data collection was performed on beamline NE3A at the Photon Factory (KEK). Data was indexed, integrated and scaled using HKL2000 [7].

2.3. Structure determination and refinement

Initial attempts to solve the LmigOBP structure by molecular replacement programs implemented in MOLREP [8], Phaser and AMoRe within the CCP4 suite [9] using any of the known OBP structures or all of them as the search models failed. After extensive trials of resolution ranges, a successful solution was obtained finally using the molecular replacement BALBES server [10] using multiple OBP structures as models. The initial model had two OBP molecules with the MR score of 3.53 and the R_{work}/R_{free} of 0.432/0.491. We excluded unstructured loops and removed disordered side chains in the density map, and the initial phase was obtained by the program REFAMC5 [11]. The program oasis [12] was used to build 70% of the main chain of the whole structure. The additional residues were rebuilt manually by COOT [13], and the model was further refined using REFMAC5 [11]. The structure was refined to 1.65 Å with an R_{work} of 18.4% and an R_{free} of 22.9%. All figures were made with Pymol [14].

3. Results

3.1. Crystal structure of LmigOBP1

Mature LmigOBP1 was successfully expressed in bacteria and purified. After trying different Tags and expression systems, only the protein purified from the periplasm produced small crystals in crystallization trials. However, further crystal optimization failed. Luckily, high-quality crystals were obtained after 6 months and diffracted to 1.65 Å (Table 1).

BLAST searches of LmigOBP1 among the solved structures in the PDB database return that the sequence identity is very low ranging from 17% to 25%. After extensive model building and refinement, the final R_{work} and R_{free} values are 0.184 and 0.229, respectively. The final model contains two LmigOBP1 molecules (residues 3–131 and 4–131), 153 water molecules and 4 PEG fragments (Table 1 and Fig. S1a). The root-mean-square deviation (r.m.s.d.) between these two LmigOBP1 was as low as 0.5 Å and structural variation was only observed in a few loop regions (Fig. S1b). The two LmigOBP1 molecules are related by a non-crystallographic 2-fold axis almost perpendicular to the plane of the page (Fig. S1a), in agreement with the self-rotation analysis (Fig. S2). Therefore, the asymmetric unit contains two monomers (Fig. S1a).

The LmigOBP1 structure has the overall fold of "classical OBPs" and is mostly helical (Fig. 1A). It exhibits a densely packed globular-shaped structure, measuring 33 Å in height, 28 Å in length, and 25 Å in width. Three conserved disulfide bonds are observed between Cys22-Cys53, Cys49-Cys100 and Cys91-Cys109, further rigidifying the structure. In LmigOBP1, seven α-helices are observed, and the seventh helix (residues 115–129, labeled α7) in the C terminus forms a wall of the internal cavity (Fig. 1B).

3.2. Protein characterization in solution

Insect OBPs may form homo- or hetero-dimers [15,16]. In LmigOBP1 structure, one asymmetric unit contains two LmigOBP1.

Table 1
Data collection and refinement statistics of LmigOBP1.

Wavelength	1.00
Space group	$P2_1$
Cell dimensions	
a, *b*, *c* (Å)	33.10, 66.04, 51.13
α, β, γ (°)	90.00, 92.41, 90.00
Resolution (Å)	50–1.65 (1.68–1.65)[a]
R_{merge} (%)	5.0 (26.0)
$I/\sigma I$	53.8 (8.8)
Completeness (%)	90.0 (50.7)
Redundancy	7.5 (7.0)
Refinement	
Resolution (Å)	30–1.65 (1.69–1.65)
No. of unique reflections	22,536 (898)
R_{work}/R_{free} (%)	18.4/22.9 (21.0/35.0)
No. of atoms (Protein/PEG/water)	2006/26/153
Average *B* factor (Protein/PEG/water, $Å^2$)	20.51/29.34/27.47
rms deviations	
Bond lengths (Å)	0.010
Bond angles (°)	1.305
Ramachandran plot (%)[b]	92.3/7.7/0/0

[a] Statistics for highest resolution shell.
[b] Residues in most favored, additional allowed, generously allowed and disallowed regions of the Ramachandran plot.

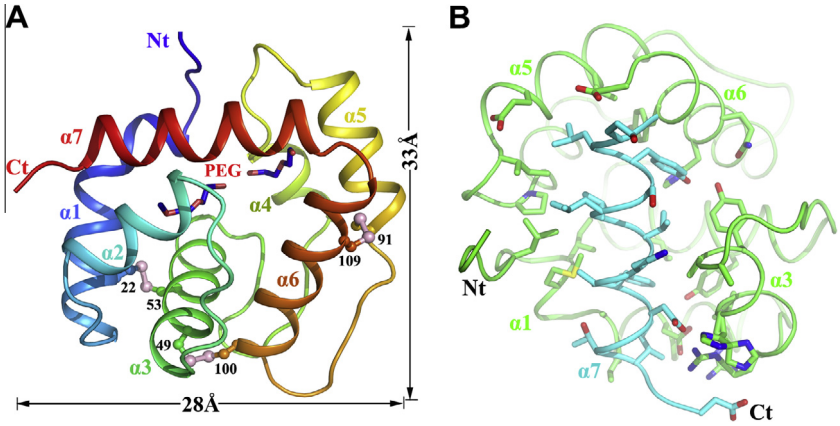

Fig. 1. Crystal structures of LmigOBP1. (A) Ribbon representation with rainbow coloring mode. Dimensions are indicated. Disulfide bonds (black numbers) are shown in ball-and-stick representations. (B) Extensive interactions between the C-terminal α7 and other parts of LmigOBP1 are illustrated. (For interpretation of the references to color in this figure legend, the reader is referred to the web version of this article.)

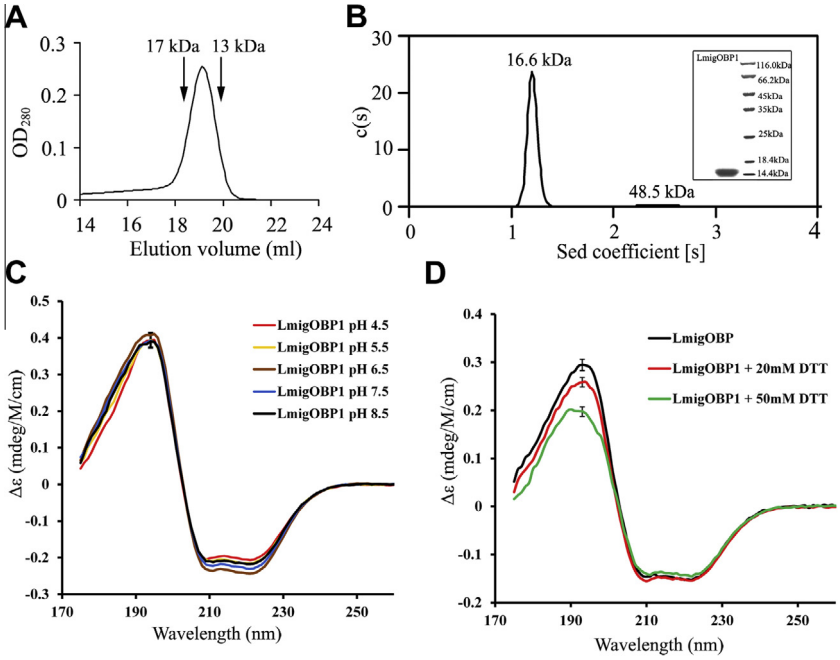

Fig. 2. The aggregation state of LmigOBP1 in solution and circular dichroism data. (A) Elution profile of LmigOBP1 in the gel filtration chromatography. (B) Analytical ultracentrifugation experiments of LmigOBP1. Continuous molar mass distribution of the protein shows a single peak with a molecular mass of 16.6 kDa (14.9 kDa theoretical mass). (C) CD spectra of LmigOBP1 at varying pH from pH 8.5 to pH 4.5. The five traces are almost indistinguishable, suggesting that the overall secondary structure is pH-independent. (D) CD spectra of LmigOBP1 in the presence of DTT. They vary greatly in the wavelength around 190 nm.

Initially, we hypothesized that LmigOBP1 remains dimer in solution [15]. This hypothesis was supported by previous studies that the closest homologs CquiOBP1 [6] and AgamOBP1 [4] were dimeric and had a long binding pocket running through the dimer. To confirm the aggregation state of LmigOBP1 in solution, we employed two methods: gel filtration and analytical ultracentrifugation. Firstly, we evaluated LmigOBP1 by size-exclusion chromatography on a calibrated Superdex-200 HR10/30 column. LmigOBP1 was eluted at 19.1 ml, corresponding to a molecular weight of ~15.8 kDa (Fig. 2A). Furthermore, the sedimentation velocity (SV) results indicated that LmigOBP1 mainly existed as a monomer (theoretical molecular weight is 14.9 kDa, Fig. 2B).

Further structural analysis shows that no hydrophobic interface is found between the two LmigOBP1 molecules in the asymmetric unit (Fig. S1a). With the exception of a few water molecule bridges, only two hydrogen bonds are observed between them. The buried surface area resulting from the dimerization contact is 238 Å^2, much less than the value of 1600 ± 400 Å^2 that is generally believed to be of physiological significance [17]. Thus, the small interface between the two LmigOBP1 molecules seems to be insufficient for dimer formation. Moreover, the free energy of assembly dissociation (ΔG^{diss}) is −9.8 kcal/mol calculated by the PISA server [18]. The negative value of the ΔG^{diss} indicates dimeric LmigOBP1 could dissociate automatically. Taken together, LmigOBP1 is monomeric in solution, greatly different from the closest homologs mosquito OBPs, in which the dimerization forms a long tunnel that traverses the interface where ligands are bound [4,6].

3.3. Structural comparison of LmigOBP1 with other known insect OBPs

A DALI search [19] of LmigOBP1 showed that AgamOBP1 [4] (Z = 14.9, r.m.s.d. = 2.1 Å) and CquiOBP1 (Z = 14.7, r.m.s.d. = 2.2 Å)

[6] as the closest OBPs. When these three structure were superimposed (Fig. 3A and B), the most significant differences were observed at the C terminus. Both AgamOBP1 and CquiOBP1 had a short C-terminal loop, which was internalized in the binding cavity. However, the C-terminal extension in LmigOBP1 was replaced by a longer additional α7 that was exposed to the solvent (Fig. 3A and B). Moreover, the corresponding residues and the hydrogen bond triad identified in CquiOBP1 and AgamOBP1 were not found in the LmigOBP1 sequence (Fig. S3). Thus, we presume that LmigOBP1 might not belong to the same subfamilies with the above two medium-chain mosquito OBPs.

Considering LmigOBP1 has an additional C-terminal helix, then we compare LmigOBP1 with two OBPs also containing the seventh helix, including AgamOBP7 (PDB ID: 3R1O) [5] and acidic form of BmorPBP (PDB ID: 1GM0) [3]. Both OBPs have low sequence identity (15%) with LmigOBP1. The structural similarity between LmigOBP1 and AgamOBP7 suggests that they may share a similar mechanism. However, the conformations of the N terminus and some loops differ significantly (Fig. 3C). The first helix of LmigOBP1 occupied the ligand (palmitic acid) position of AgamOBP7 [5] (Fig. S4a). Moreover, AgamOBP7 had the fourth disulfide bond, which linked the seventh helix to the OBP scaffold (Fig. 3C). For BmorPBP, it has a significant structural difference ($Z = 8.7$, r.m.s.d. = 3.4 Å) compared with LmigOBP1. Moreover, the seventh helix of BmorPBP was formed at pH 4.5 and located in the protein core (Fig. 3D). However, the α7 in LmigOBP1 does not occupy the cavity, but forms a wall of the cavity.

3.4. The ligand-binding pocket of LmigOBP1 differs from that of mosquito OBPs

Pentadecanol and 2-pentadecanone were best candidate ligands for LmigOBP1 [20]. Then we make efforts to obtain the complex structure of LmigOBP1 with ligands, but the result was unsuccessful. Therefore, we studied the binding pocket by structural analysis and bioinformatics calculation.

Generally, there are two possible binding pockets for ligands, one is the inner largest cavity, and the other is the cavity between helices α4 and α5. Most of insect OBPs bind ligands in the former, while the latter might be universal among mosquito OBPs [6]. Sequence alignment (Fig. S3) shows that mosquito OBPs have the highest sequence identity to LmigOBP1 among the structure-solved insect OBPs, raising the possibility that LmigOBP1 also might bind ligands like CquiOBP1. Superimposition of LmigOBP1 with CquiOBP1–ligand complex structure [6] implied that residues Val88 and His89 in the helix α5 of LmigOBP1 directly crashed the ligand in the CquiOBP1–ligand complex (Fig. 4A). Especially, compare to the corresponding small residue Gly92 in CquiOBP1, the larger hydrophobic residue Val88 in LmigOBP1 forms an extensive network of van der Waals contacts with Leu69, Phe67, Tyr110, Leu73, Val76 and Ile80. Moreover, the side chain of His89 also forms a hydrogen bond with the side chain of Lys92, further fixing the overall conformation. Therefore, the helix α5 in LmigOBP1 moves 2.9 Å closer to the helix α4 to reduce the putative cavity compared with that in CquiOBP1 (Fig. 4A). Furthermore, cavity calculation shows no cavity exist between helices α4 and α5 in LmigOBP1 (Fig. 4B). Thus, it might be impossible to bind ligands in the position like CquiOBP1.

The position of the binding pocket was further verified by carrying out flexible molecular docking. We found that the binding energy were −5.90 kcal/mol for pentadecanol and −6.20 kcal/mol for 2-pentadecanone when the ligands were located in the inner cavity of LmigOBP1. However, the binding energy proved very high when these two ligands were artificially docked in the position between helices α4 and α5. Taken together, these results suggest

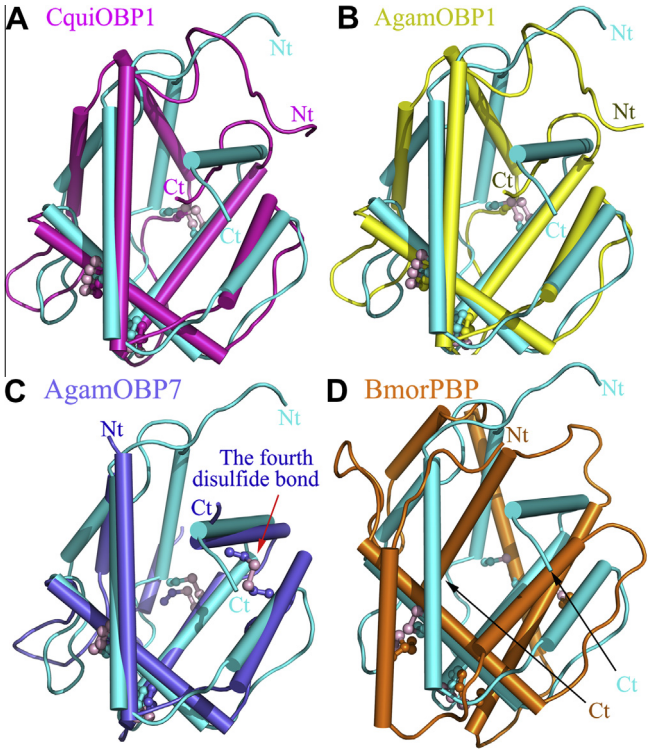

Fig. 3. Superimposition of LmigOBP1 (cyan) on selected OBPs. (A) CquiOBP1 (PDB ID: 3OGN, magenta). (B) AgamOBP1 (PDB ID: 2ERB, yellow). (C) AgamOBP7 (PDB ID: 3R1O, blue). (D) BmorPBP (PDB ID: 2FJY, orange). Conserved disulfide bonds (lightpink) are shown in ball-stick modes. (For interpretation of the references to color in this figure legend, the reader is referred to the web version of this article.)

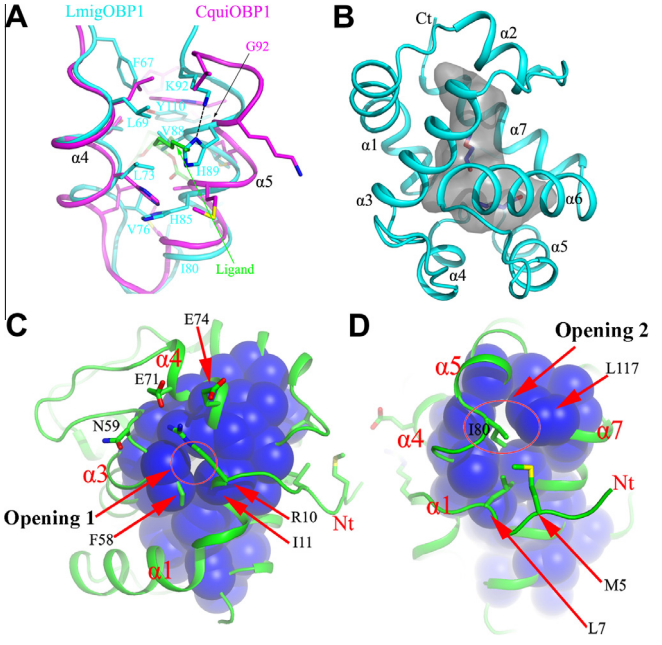

Fig. 4. The ligand-binding pocket and the two openings in LmigOBP1. (A) Superimposition of LmigOBP1 (cyan) on CquiOBP1 (magenta)–ligand (green) complex. Hydrogen bonds are shown in black dashed lines. Residues Val88 and His89 in helix α5 of LmigOBP1 directly crash the ligand from the CquiOBP1–ligand complex. (B) LmigOBP1 has an "L" shaped cavity, which might be preferable to bind linear aliphatic ligands. (C) The opening 1 is composed of α1, α3, and α4, the N-terminus is locked by the electrostatic interaction and hydrophobic interaction. (D) The opening 2 is invisible when shown as surface mainly because of the obstruction of the residues Met5, Leu7 and Ile80. (For interpretation of the references to color in this figure legend, the reader is referred to the web version of this article.)

that the ligand-binding mechanism of mosquito OBPs probably does not apply to LmigOBP1, that is, the ligands probably interact with LmigOBP1 at the inner largest cavity.

3.5. LmigOBP1 binding cavity

An "L" shaped cavity was observed at the center of LmigOBP1 (Fig. 4B), and it had a volume of 830 ± 12 Å^3, which was enough to adopt long carbon chain aliphatic alcohols or ketones up to 15 carbon atoms [20]. The cavity walls are predominantly hydrophobic residues. Other than these residues, there are several hydrophilic residues, such as Ser60, Asn75, Glu72 and His107 (Fig. S5). The predominantly hydrophobic and additional hydrophilic internal cavity of LmigOBP1 provides all possible interactions for ligand binding.

In LmigOBP1, there are two openings in the structure (Fig. 4C and D). The visible small opening (the opening 1) of the binding cavity is created by helices α1, α3, and α4. This opening is about 3.5 and 5.0 Å in width and height, partly hindered by residues Arg10 and Ile11 in helix α1 sterically (Figs. S6 and 4C). Moreover, residue Arg10 forms electrostatic interactions with Glu71 and Glu74. Additionally, residue Phe58 exhibits a hydrophobic interaction with the side chain of Ile11 (Fig. S4a). These interactions fix the side chain of Arg10 and Ile11. The binding experiments also showed that the mutant R10A/I11A obviously inhibited the binding ability of LmigOBP1 (Fig. S7a–b and Table S1). Therefore, the helix α1 is important for the ligand binding. If the structure rotates 90° along the *Y* axis, another opening (the opening 2) appears (Fig. 4D). It is invisible when shown as surface, mainly because of the obstruction of residues Met5, Leu7, and Ile80.

3.6. The unique C-terminal helix α7 of LmigOBP1

In LmigOBP1, the α7 exposed to the solvent, formed a wall of the cavity, and wrapped around the protein surface (Fig. S8). The α7 structurally resembles that in AgamOBP7, a class of OBPs which possesses eight cysteines [5]. However, different from the fixation by the fourth disulfide bridge in AgamOBP7 (Fig. 3C), the α7 in LmigOBP1 forms strong interactions with the LmigOBP1 core through a number of hydrogen bonds, salt bridges, and hydrophobic interactions (Fig. 1B). And the interface area reaches 873.4 Å^2. Taken together, the structural feature and large interaction surface make the binding of α7 to the LmigOBP1 core tightly so that the entry of ligand into the cavity from the C terminus may be very difficult.

3.7. LmigOBP1 structure is independent of changes in pH

It has been shown that changes in pH induce conformational change in insect OBPs, a mechanism to regulate ligand binding and release [3,4,6,21–24]. To verify whether LmigOBP1 obey this mechanism, circular dichroism (CD) experiments were conducted from pH 8.5 to pH 4.5. The CD spectra of LmigOBP1 at different pH (Fig. 2C) were similar to each other. In contrast, disruption of the disulfide bonds by high concentration DTT greatly affected the secondary structure (Fig. 2D). The pH experiments' result indicated that no distinguishable changes were found on the overall secondary structure of LmigOBP1. These findings further suggest that LmigOBP1 has a prominent different mechanism from BmorPBP, although all of them have long C-terminal tails. Therefore, it is currently believed that changes in pH don't trigger conformational change for LmigOBP1.

Moreover, LmigOBP1 does not have the hydrogen bond triad as observed in AgamOBP1 and CquiOBP1. The hydrogen bond triad was identified in the C terminal last residue (Val/Ile), the residues positioned at the first helix (His) and the third helix (Tyr) at neutral pH. The hydrogen bond triad was proposed as a pH-sensing "lock" clamping the C-terminal loop onto the bound substrate [6]. Structural alignment shows that the corresponding residues in LmigOBP1 are Phe125-Asp19-Tyr50 (Figs. S3 and S4b). It is well-known that only histidine side chain would greatly change its charge from pH 8.5 to pH 4.5. However, there is no histidine residue in the corresponding residues of LmigOBP1. Thus, ligand binding to LmigOBP1 might not regulated by changes of pH falling from pH 8.5 to 4.5.

4. Discussion

Our results imply that three conserved disulfide bonds play an important role in stabilizing the protein scaffold. To further confirm it, we used CD experiments in different DTT concentration. The spectrum of LmigOBP1 in the presence of 50 mM DTT was greatly different from that without DTT (Fig. 2D). Furthermore, binding experiments revealed that high concentration of DTT decreased the binding ability of 1-NPN to LmigOBP1 (Fig. S7c). In summary, these results demonstrated that the disulfide bonds play a crucial role in maintaining LmigOBP1 function.

In this study, we found that LmigOBP1 differed greatly from the closest homologs mosquito OBPs, in the oligomeric state, hydrogen bond triad, ligand entry and release mechanism. Moreover, the unique structure in LmigOBP1 mainly exists in the seventh α7, and most of α7 is embedded in the surface. And the N-terminal helix α1 participates in electrostatic interaction and hydrophobic interaction with surrounding residues in helices α3 and α7. Thus the helices α1 and α7 are relatively fixed and might not be involved in the ligand entry and release. Compare to the structure of AgamOBP7–ligand complex, the remarkable differences in LmigOBP1 are mainly reflected in the loop connecting helices α4 and α5, which is stabilized by the N-terminal loop (Fig. 4D). Thus, we propose that the N-terminal loop and the loop between helices α4 and α5 might function as "lid" to switch on the opening 2 to control the ligand entry and release. This further suggests that LmigOBP1's unique feature makes it different from any other insect OBPs in ligand entry and release mechanism.

It is widely accepted that insect OBPs have a rather versatile scaffold owing to their diverse lengths, positions, orientations of helices, and variety of loops. Therefore, these significant structural differences make the insect OBPs display cavity shapes and different openings to accommodate diverse ligands. The "L" shaped cavity in LmigOBP1 structure possibly could explain its preference in binding linear aliphatic compounds in a length-dependent manner.

Acknowledgments

We thank Prof. Jiafu Long for analytical ultracentrifugation experiments and Prof. Yongjun Zhang for fluorescence binding assay. This work was supported by National Basic Research Program of China (973 Program, 2011CB965304), National Natural Science Foundation of China (31370720, 31222032, 31300135 and 11179021).

Appendix A. Supplementary data

Supplementary data to this article contains supplementary experimental procedures and supplementary figures S1–S8 and Table S1. Supplementary data associated with this article can be found, in the online version, at http://dx.doi.org/10.1016/j.bbrc.2014.12.048.

References

[1] R.G. Vogt, L.M. Riddiford, Pheromone binding and inactivation by moth antennae, Nature 293 (1981) 161–163.

[2] B.H. Sandler, L. Nikonova, W.S. Leal, J. Clardy, Sexual attraction in the silkworm moth: structure of the pheromone-binding-protein-bombykol complex, Chem. Biol. 7 (2000) 143–151.
[3] R. Horst, F. Damberger, P. Luginbuhl, P. Guntert, G. Peng, L. Nikonova, W.S. Leal, K. Wuthrich, NMR structure reveals intramolecular regulation mechanism for pheromone binding and release, Proc. Natl. Acad. Sci. U.S.A. 98 (2001) 14374–14379.
[4] M. Wogulis, T. Morgan, Y. Ishida, W.S. Leal, D.K. Wilson, The crystal structure of an odorant binding protein from *Anopheles gambiae*: evidence for a common ligand release mechanism, Biochem. Biophys. Res. Commun. 339 (2006) 157–164.
[5] A. Lagarde, S. Spinelli, M. Tegoni, X. He, L. Field, J.J. Zhou, C. Cambillau, The crystal structure of odorant binding protein 7 from *Anopheles gambiae* exhibits an outstanding adaptability of its binding site, J. Mol. Biol. 414 (2011) 401–412.
[6] Y. Mao, X. Xu, W. Xu, Y. Ishida, W.S. Leal, J.B. Ames, J. Clardy, Crystal and solution structures of an odorant-binding protein from the southern house mosquito complexed with an oviposition pheromone, Proc. Natl. Acad. Sci. U.S.A. 107 (2010) 19102–19107.
[7] Z. Otwinowski, W. Minor, Processing of X-ray diffraction data collected in oscillation mode, in: J. Charles, W. Carter, R.M. Sweet (Eds.), Methods in Enzymology, Academic Press, New York, 1997, pp. 307–326.
[8] A. Vagin, A. Teplyakov, Molecular replacement with MOLREP, Acta Crystallogr. D Biol. Crystallogr. 66 (2010) 22–25.
[9] M.D. Winn, C.C. Ballard, K.D. Cowtan, E.J. Dodson, P. Emsley, P.R. Evans, R.M. Keegan, E.B. Krissinel, A.G. Leslie, A. McCoy, S.J. McNicholas, G.N. Murshudov, N.S. Pannu, E.A. Potterton, H.R. Powell, R.J. Read, A. Vagin, K.S. Wilson, Overview of the CCP4 suite and current developments, Acta Crystallogr. D Biol. Crystallogr. 67 (2011) 235–242.
[10] F. Long, A.A. Vagin, P. Young, G.N. Murshudov, BALBES: a molecular-replacement pipeline, Acta Crystallogr. D Biol. Crystallogr. 64 (2008) 125–132.
[11] G.N. Murshudov, P. Skubak, A.A. Lebedev, N.S. Pannu, R.A. Steiner, R.A. Nicholls, M.D. Winn, F. Long, A.A. Vagin, REFMAC5 for the refinement of macromolecular crystal structures, Acta Crystallogr. D Biol. Crystallogr. 67 (2011) 355–367.
[12] L.J. Wu, T. Zhang, Y.X. Gu, C.D. Zheng, H.F. Fan, Direct-method SAD phasing of proteins enhanced by the use of intrinsic bimodal phase distributions in the subsequent phase-improvement process, Acta Crystallogr. D Biol. Crystallogr. 65 (2009) 1213–1216.
[13] P. Emsley, B. Lohkamp, W.G. Scott, K. Cowtan, Features and development of Coot, Acta Crystallogr. D Biol. Crystallogr. 66 (2010) 486–501.
[14] L. Schrödinger, The PyMOL molecular graphics system, Version 1.3, 2010.
[15] L. Ban, A. Scaloni, C. D'Ambrosio, L. Zhang, Y. Yahn, P. Pelosi, Biochemical characterization and bacterial expression of an odorant-binding protein from *Locusta migratoria*, Cell. Mol. Life Sci. 60 (2003) 390–400.
[16] H. Qiao, X. He, D. Schymura, L. Ban, L. Field, F.R. Dani, E. Michelucci, B. Caputo, A. della Torre, K. Iatrou, J.J. Zhou, J. Krieger, P. Pelosi, Cooperative interactions between odorant-binding proteins of *Anopheles gambiae*, Cell. Mol. Life Sci. 68 (2011) 1799–1813.
[17] L. Lo Conte, C. Chothia, J. Janin, The atomic structure of protein–protein recognition sites, J. Mol. Biol. 285 (1999) 2177–2198.
[18] E. Krissinel, K. Henrick, Inference of macromolecular assemblies from crystalline state, J. Mol. Biol. 372 (2007) 774–797.
[19] L. Holm, P. Rosenström, Dali server: conservation mapping in 3D, Nucleic Acids Res. 38 (2010) W545–W549.
[20] Q.Y. Jiang, W.X. Wang, Z. Zhang, L. Zhang, Binding specificity of locust odorant binding protein and its key binding site for initial recognition of alcohols, Insect Biochem. Mol. Biol. 39 (2009) 440–447.
[21] N.R. Leite, R. Krogh, W. Xu, Y. Ishida, J. Iulek, W.S. Leal, G. Oliva, Structure of an odorant-binding protein from the mosquito Aedes aegypti suggests a binding pocket covered by a pH-sensitive "Lid", PLoS ONE 4 (2009) e8006.
[22] H. Wojtasek, W.S. Leal, Conformational change in the pheromone-binding protein from *Bombyx mori* induced by pH and by interaction with membranes, J. Biol. Chem. 274 (1999) 30950–30956.
[23] M.E. Pesenti, S. Spinelli, V. Bezirard, L. Briand, J.C. Pernollet, M. Tegoni, C. Cambillau, Structural basis of the honey bee PBP pheromone and pH-induced conformational change, J. Mol. Biol. 380 (2008) 158–169.
[24] F.F. Damberger, Y. Ishida, W.S. Leal, K. Wuthrich, Structural basis of ligand binding and release in insect pheromone-binding proteins: NMR structure of Antheraea polyphemus PBP1 at pH 4.5, J. Mol. Biol. 373 (2007) 811–819.